# Analysis of River Flow Velocity Measurement Using the Large-Scale Particle Image Velocimetry Method

**Bashit, N.,*** **Sasmito, B., Maladzi, H. S., Haryadi, S., Prasetyo, Y. and Yuwono, B. D.**
Department of Geodetic Engineering, Faculty of Engineering, Diponegoro University, Semarang, Indonesia
E-mail: nurhadi.bashit@live.undip.ac.id*
**Corresponding Author*

**DOI: https://doi.org/10.52939/ijg.v21i9.4449**

**Abstract**
*Large-scale particle image velocimetry (LSPIV) can analyze river flow velocity measurement. LSPIV can be performed using either a UAV or terrestrial photogrammetry, but it is important to understand the river flow velocity measurement results from both methods. This study examines the river flow velocity measurement of the Mungkung River water flow in the Mungkung Bridge, Sragen Regency, using an unmanned aerial vehicle (UAV) and terrestrial photogrammetry. The velocity of river water flow will be measured using the large-scale particle image velocimetry (LSPIV) method and orthorectification with the RIVeR application. UAV orthorectification at each height of 20 m, 30 m, and 50 m. The results of measuring the velocity of river currents using the UAV LSPIV method obtained a range of results between 0.1 - 0.7 m/s with a flight height of 20 meters, 0-0.7 m/s at a UAV flight height of 30 meters, and 0.0-0.8 m/s with a UAV flight height of 50 meters, while terrestrial photogrammetry has a velocity value with a range of value variations of 0-0.7 m/s. Meanwhile, preliminary validation measurement obtained a river flow velocity of 0.393 m/s, and the River Basin Organization of Bengawan Solo River data using a current meter produced a velocity value of 0.375 m/s.*

**Keywords:** Large-Scale Particle Image Velocimetry, RIVeR, River Flow, Terrestrial Photogrammetry, Unmanned Aerial Vehicle

## 1. Introduction

River flow measurement is a common river hydraulic measurement used as the primary parameter for understanding river dynamic characteristics. Measuring the velocity of river flow is very important because it defines hydrological characteristics, serves as a guideline for upstream management plans and river springs, and helps in understanding the impacts of climate change. Flood disaster mitigation can be detected by accurately measuring river flow velocity and can manage water resources, riverbank erosion control, and sedimentation [1]. The distribution of flow velocities over large areas undoubtedly contributes to the understanding of natural phenomena and provides a better basis for decision-making [2]. Traditionally, velocity measurements are performed with mechanical or electromagnetic current meters [3], acoustic wave-transmitter equipment, and other instruments: Acoustic Doppler Current Profilers (ADCPs), Acoustic Doppler Velocimeters (ADVs), or Surface Velocity Radar (SVR) [4] and [5]. River flow velocity measurements can be carried out using various types of process measurement instruments that provide good spatial and temporal resolution but are expensive to maintain [6]. Calculating the velocity of stream water currents using such equipment requires a minimum water depth and repeated measurements, endangers the equipment operator, and cannot reach distant and vegetated areas [7]. Current meters can obtain data in real time, but their use requires going directly to the field.

However, conventional methods have the disadvantage of requiring long and expensive data acquisition times, as well as requiring highly specialized personnel [8]. Along with the development of technology, the method of measuring river flow velocity has undergone rapid development. Several studies have proven a flexible, efficient, and safe method using remote sensing. The development of methods utilizing image velocimetry approaches combined with remote sensing methods to overcome inconveniences in measuring surface velocities is urgently required [9]. The photogrammetry technology utilizes cameras that enable the cheap and easy acquisition of photo or video data over large areas.

The camera is placed on the bridge to obtain photos and videos of the river surface, which are analyzed to calculate the river flow surface. During the image capture phase of image velocimetry, the camera ideally has to stay at a fixed and elevated position to conduct an adequate survey of the area of interest [10]. This technique allows us to know the characteristics of the river water surface to analyze the river flow velocity at certain locations in the river.

The image velocimetry technique is obtained from photo and video data based on the movement of visible particles recorded and two-dimensional velocity calculations [11]. Developments have made Particle Image Velocimetry (PIV) usable in aquatic environments on a large-scale. The imaging-based flow diagnostic method known as particle image velocimetry (PIV) relies on seeding fluid flows with microscopic tracer particles and identifying the motions associated with the tracer particles to determine fluid velocities [12]. This large-scale application of Particle Image Velocimetry (PIV) is often called large-scale particle image velocimetry (LSPIV). The river flow velocity will be estimated using photogrammetry techniques with the large-scale particle image velocimetry (LSPIV) method utilizing tracking on objects or features that float on the river and are visible in a set of photos processed from video and then used in calculating the speed of river flow [13]. In this LSPIV method, the parameter taken into account in the speed of river flow is frames per second (fps), which is modeled using the movement of pixels/frames and then converted into units of speed in meters per second after GCP binding [14].

The interrogation area (IA) used greatly affects the calculation of velocity with LSPIV because the use of a small IA produces vectors with high resolution, but this also increases noise and can make errors in correlation calculations [15].The use of Ground Control Points (GCP) and Independent Check Points (ICP) in the LSPIV method is to convert units in the form of frames per second to meters per second and orthorectification. However, the ground control points utilized for image calibration and orthorectification, as well as the orthogonal images needed for additional processing, have a significant impact on LSPIV [16]. The LSPIV method requires a minimum of four GCPs spread on both sides of the river [17]. In research conducted by Sharif in 2022, six GCPs and three ICPs were used [4]. In 2017, Patalano conducted research on measuring river flow velocity using the LSPIV method using the Matlab-based RIVeR application, the stages of which consisted of capturing images extracted from videos, then entering camera calibration parameters, and then carrying out image stabilization. After obtaining a stable photo, image enhancement is carried out and velocity vector calculation is done using the interrogation area, and the outlier vector is sorted out with the PIVlab application. After the vector is obtained, orthorectification and cross-section drawing are then carried out to obtain river current velocity data in units of m/s [7]. The current development of the LSPIV method has been widely applied to measure the surface of river flow in locations with low/normal flow conditions [18]. Terrestrial photogrammetry has the disadvantage of limited recording area coverage. Therefore, river flow velocity measurement can utilize advances in unmanned aerial vehicle (UAV) technology [10]. The use of Unmanned Aerial Vehicles (UAVs) allows for low-cost analysis of river flow velocity in difficult-to-access locations [19]. State-of-the-art techniques for the characterization of surface water processes allow for performing flow measurements at selected and accessible locations in watershed drainage networks [20].

This study examines the river flow velocity measurement of the Mungkung River flow in the Mungkung Bridge, Sragen Regency, using an unmanned aerial vehicle (UAV) and terrestrial photogrammetry. The camera was placed on a bridge to observe the river surface, while the UAV was used at three different heights. Both measurements used large-scale particle image velocimetry to estimate surface river flow velocity. The estimation results were compared with field validation data.

## 2. Methodology

This research was conducted in Mungkung River, Sragen Regency, Indonesia (Figure 1), using a DJI Phantom 4 Standard UAV and a Canon 2000D DSLR camera. Mungkung River is one of the tributaries of Bengawan Solo River, which springs from Mount Lawu. This river has a length of 31.21 km with a watershed area of 184.70 km² [21]. The Mungkung River in Sragen Regency becomes the natural boundary of the Sragen and Sidoharjo subdistricts in Sragen Regency. The location of the air flow measurement is located in shallow water. Data in the form of benchmark coordinate data as a reference, ground control point data as orthorectification control points, independent check point data as control points for testing orthorectification results, camera calibration data, and river object video data. The data was taken as primary data at the research location in Mungkung River, Sragen Regency, which can be seen in Figure 2.

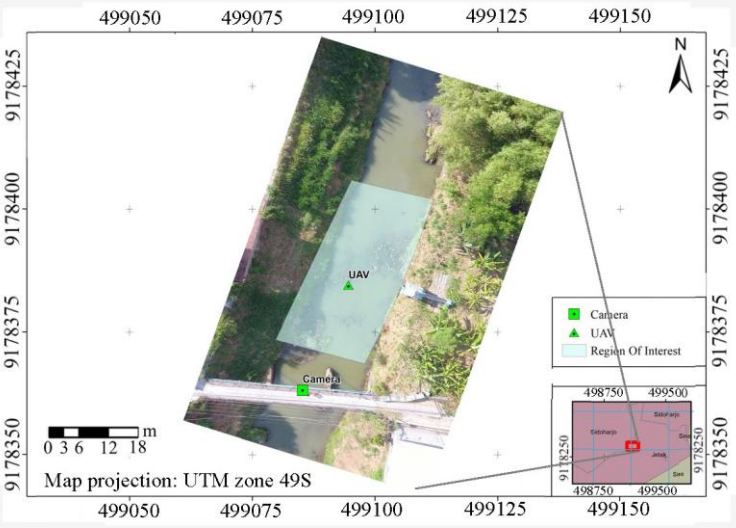


**Figure 1:** River flow velocity test site

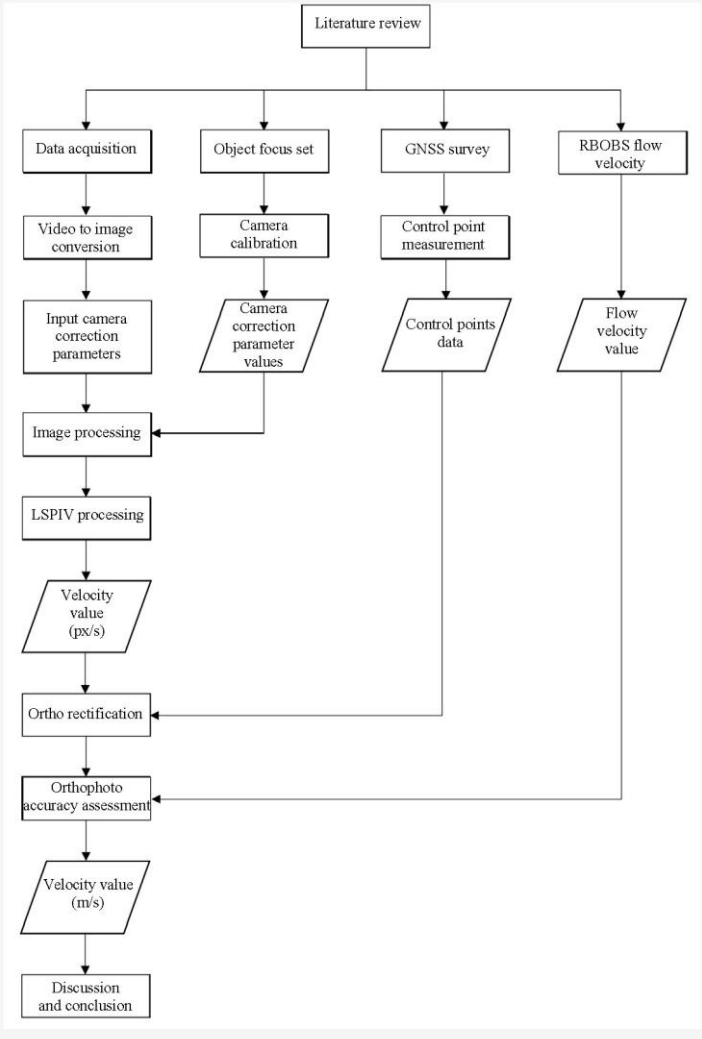


**Figure 2:** River flow velocity measurement

The equipment used in this research is a laptop, a Sokkia IM-52 Total Station set and its equipment, a Topcon HiPer II and HiPer SR GNSS, and a Canon 2000D DSLR camera with a camera tripod. Topographic surveys and simultaneous flow river measurements by the LSPIV technique [5]. The software used in this research includes PIVlab and RIVeR. The processing phase was conducted through the freely available open-source PIVlab software [22], developed in the MATLAB environment. RIVeR (Rectification of Image Velocity Results) is an application developed by A. Patalano and co-workers in the Center for Water Research and Technology (CETA) at the National University of Cordoba, Argentina, in 2013 [8].

This research begins with UAV and camera data collection to compare the results of river flow surface measurements. The camera is calibrated to obtain camera correction parameter values for image preprocessing. UAV and camera measurements are controlled using GNSS measurements to allow for orthorectification. Initial processing begins with video extraction into photo frames, which are then processed together with camera correction parameters. Processing is continued using LSPIV to obtain velocity values (px/s), which are then processed for orthorectification tested using GNSS data. Orthorectification data processing to obtain river flow velocity (meters/s).

*2.1 Large-Scale Particle Image Velocimetry*

Particle Image Velocimetry, or PIV, is one method that can be used to measure velocity in a fluid flow. LSPIV is one of the most widely used optical techniques [20] and is based on four main phases: (i) seeding and recording; (ii) image pre-processing; (iii) image processing; and (iv) image post-processing. PIV is based on paired images with image enhancement, image evaluation, and post-processing [11]. PIV uses image processing of photos or recordings to determine the amount of instantaneous velocity in the fluid flow and calculates the lighting reflection of the speed of movement of particles (seeders) captured by the sensor with Equation 1:

$$D_l = X_e - X_o$$

Equation 1

Where:

$D_l$ is the displacement vector
$X_e$ is the coordinates at the starting point
$X_o$ is the coordinates projection at the end point

The displacement with units of time is calculated by the velocity formula based on Equation 2:

$$V_l = \frac{D_l}{\Delta t}$$

Equation 2

Where:

$D_l$ is the displacement vector
$\Delta t$ is the time between paired images

PIV flow velocity displacement measurements are taken at the interrogation area in the specified image pair [11]. The photographic or recorded image files are then read and processed to obtain the magnitude and direction of velocity at the particle/seeder location [13]. The development of PIV for large areas can use large-scale particle image velocimetry, which can implement transformation and orthorectification on photos. Orthorectification works by manipulating oblique images so that each pixel is transformed into real coordinates/ground coordinates [4]. The Interrogation Area (IA) used in the image processing was 128x128 pixels for the first pass, then followed by 64x64 and 32x32 pixels for the second and third passes, all with a total overlap within the IA of 50%. When the IA is too small, it will cause the vector velocity to be too big and increase the noise and error [23].

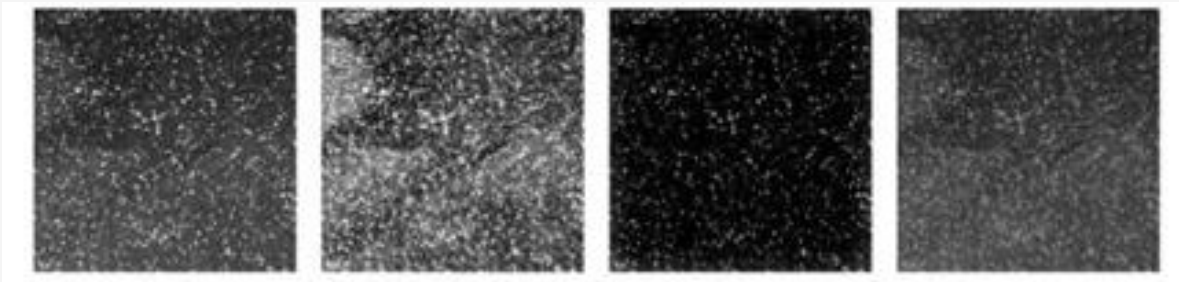

(a) (b) (c) (d)

**Figure 3:** The difference and result from image enhancement on the PIVlab: (a) original, (b) CLAHE, (c) high-pass, (d) intensity capping [24]

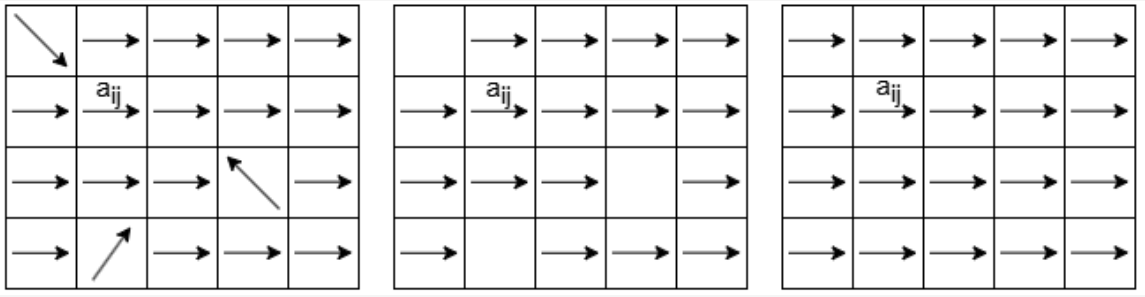


**Figure 4:** Data correction process in the LSPIV post processing:
(a) before vector correction, (b) after outlier removal, (c) after interpolation [25]

Videos obtained from the site need to be enhanced to make the particle or seeder that was carried away by the water evident. The main key of the image enhancement is to transform the pixel intensity value in the entire frame so the particles or seeds on the water surface contrast visually with the background [20]. There are 3 image enhancement methods on PIVlab, such as Contrast Limited Adaptive Histogram (CLAHE), intensity high-pass filter, and intensity capping (Figure 3). The CLAHE method optimized the area that has low intensity and high intensity independently, so this technique is suitable for the pictures that have variation levels of high intensity [4].

A high-pass filter is used to remove the objects that have low frequency on the photo background and maintain the high-frequency object (seeder/tracer). This method will work well in the river with rock, sand, and vegetation [24]. Intensity capping is used to reduce the influence, where a very bright feature has to be reduced in the entire frame. There is no formal technique for PIV image enhancement, so trial was needed to choose the right methods. In the LSPIV analysis, it was recommended to use CLAHE [7].

Post-processing illustrates in Figure 4 is a process that needs to be done wherein, in post-processing, the outlier detection is carried out with the purpose of getting a reliable river flow velocity estimation [22]. On PIVlab, outlier detection has to be done manually and visually to determine the minimum and maximum value of the velocity. After removing the outlier, the data emptiness will then be filled with the correct vector from neighboring value interpolation.

*2.2 Research Preparation*

*2.2.1 Camera calibration*

The distortion characteristics, such as tangential and radial distortion, as well as other lens parameters, such as the image's fiducial center point, focal length, and primary points (*cx* and *cy*), are determined by camera calibration [14]. The camera calibration process was performed using the on-the-job calibration method using checkerboard paper with a pattern size of 20 mm.

*2.2.2 Ground Control Point and Independent Check Point*

Control point data was acquired using a total station standing on each benchmark referring to GNSS measurements with GCP and ICP locations as shown in Figure 5. Control point data is used as GCP for orthorectification processing and ICP for data quality testing of orthorectification results. GCP and ICP measurements were carried out with 6 times iterated measurements for GCP and 4 times iterated measurements for ICP.

*2.3 Data Acquisition*

The acquisition process was carried out on Friday, July 21, 2023, at 14:53 local time (GMT+7). The acquisition was carried out past 12:00 local time (GMT+7) to avoid excessive lighting/illumination. The timing was also chosen to avoid a lot of shadows falling on the object area. This kind of data acquisition was used to minimize the distortion and made the calculation on the application produce a better result.

*2.3.1 UAV data acquisition*

UAV data acquisition utilized a DJI Phantom 4 Standard positioned at an angle of 0°, resulting in a 90° angle relative to the surface of the study area. The camera parameter can be seen in Table 1. When frames are taken by drones (e.g., from a height of about 20 m and above), the difference in the z-coordinates of the GCPs can be neglected, assuming that the GCPs lie on the plane of the river surface [17].

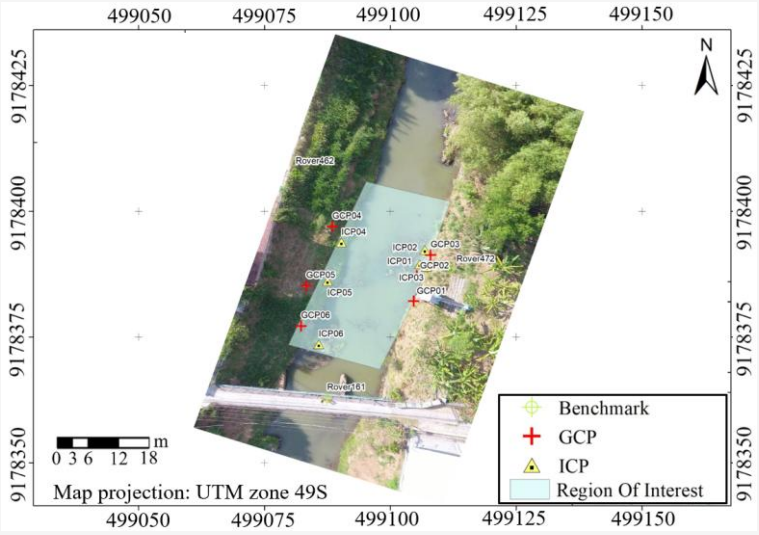


**Figure 5:** Control point position

**Table 1:** UAV configuration

| Number | Information | Description |
|---|---|---|
| 1 | UAV | DJI Phantom 4 Standard |
| 2 | Video Resolution | 1920x1080px |
| 3 | Flight height | 20, 30, and 50 meter |
| 4 | frame rate | 30fps |
| 5 | ISO | 1600 |
| 6 | Aperture | F5.6 |

**Table 2:** DSLR camera configuration

| Number | Information | Description |
|---|---|---|
| 1 | Digital Single Lens Reflex | Canon 2000D |
| 2 | Video Resolution | 1920x1080px |
| 3 | Tilt Angle | 60° |
| 4 | frame rate | 30fps |
| 5 | ISO | 400 |
| 6 | Aperture | F5.6 |

*2.3.2 DSLR camera data acquisition*

The camera was mounted on a tripod at an angle of 60° from the nadir point in the study area. The DSLR configuration can be seen at Table 2.

*2.3.4. Orthorectification*

PIVlab uses input data in the form of raw video so that the video is not yet upright and produces river flow velocity values in pixel/s values. Orthorectification is performed in RIVeR software using the flow velocity data that has been processed with PIVlab with the aim of obtaining changes in river flow velocity in m/s. Orthorectification uses GCP coordinates and camera calibration values to produce an upright river flow velocity model, which is then carried out in an accuracy assessment process using ICP points. PIVlab uses a boundary value solver as an interpolation algorithm, extrapolating missing data from the neighboring nodes through vertical, horizontal, and diagonal connections [5].

*2.3.5 Preliminary Validation Data Acquisition*

Validation data collection was carried out using a dry leaf object that was washed away within a distance of 5 meters, and the duration was measured using a stopwatch. The material was chosen to float on the surface of the river and provide strong contrast with the background. The object used in this validation was a dry leaf, which was floated at a measured distance of 5 meters with 60 repetitions. Preliminary validation is carried out in a location that is not disturbed by other objects.

## 3. Results and Discussion

### *3.1 GNSS result*

Benchmark coordinate measurement results using GNSS with Base on TTG 1116 located in Krikilan Village, Masaran Subdistrict, Sragen Regency, at the research location. The GNSS measurement results are displayed in topocentric Cartesian coordinates in UTM zone 49s and the orthometric height system in Table 3. Based on the GNSS processing results, it can be seen that the observation results provide a standard deviation value of less than 5 mm, from which it can be concluded that the observation meets the technical specifications of the 2nd order control net observation.

### *3.2 Camera Calibration Result*

The camera calibration process produces focus parameter values (*fx*, *fy*), center point (*cx*, *cy*), radial distortion values (*k1*, *k2*, *k3*), and tangential distortion values (*p1*, *p2*) in pixels. Error values are displayed in millimeters with details, as in Table 4 and Table 5.

### *3.3 Orthorectification Result*

#### *3.3.1 UAV orthorectification result*

The results of the orthorectification test obtained RMSE values of 0.28 m at a flying height of 20 meters, 0.294 m at a flying height of 30 meters, and 1.879 m at a flying height of 50 meters, as can be seen in Tables 6 to 8, respectively. Determination of the map class is done by calculating the RMSE of the ICP test with the formula CE90 = 1.5175×RMSE Horizontal, resulting in a value of 0.425 at a flying height of 20 meters, which is included in the 1:1,000 third-class scale map; 0.447 at a flying height of 30 meters, which is included in the 1:1,000 third-class scale map; and 2.851 at a flying height of 50 meters, which is included in the 1:10,000 second-class scale map.

**Table 3:** Result of GNSS observation

| Name | Grid Northing (m) | Grid Easting (m) | Elevation (m) | Std Dev N (m) | Std Dev E (m) | Std Dev U (m) | Std Dev Hz (m) |
|---|---|---|---|---|---|---|---|
| Base 165 | 9175172.832 | 494426.786 | 118.169 | 0 | 0 | 0 | 0 |
| Rover 161 | 9178362.772 | 499087.485 | 104.896 | 0.002 | 0.002 | 0.006 | 0.003 |
| Rover 462 | 9178407.698 | 499081.246 | 104.567 | 0.002 | 0.002 | 0.005 | 0.003 |
| Rover 472 | 9178388.724 | 499111.974 | 102.459 | 0.002 | 0.002 | 0.005 | 0.003 |

**Table 4:** DJI phantom 4 standard camera calibration result

| Parameter | Definition | Value (px) |
|---|---|---|
| *fx* | X Axis *Focal Length* Value | 976.009 |
| *fy* | Y Axis *Focal Length* Value | 731.930 |
| *cx* | X Axis *Principal Points* Value | 871.310 |
| *cy* | Y Axis *Principal Points* Value | 577.159 |
| *k1* | Radial Distortion Value | -0.009 |
| *k2* | Radial Distortion Value | 0.049 |
| *k3* | Radial Distortion Value | 0.039 |
| *p1* | Tangential Distortion Value | 0.001 |
| *p2* | Tangential Distortion Value | 0.0001 |

**Table 5**: Canon 2000D camera calibration result

| Parameter | Definition | Value (px) |
|---|---|---|
| *fx* | X Axis *Focal Length* Value | 896.459 |
| *fy* | Y Axis *Focal Length* Value | 922.420 |
| *cx* | X Axis *Principal Points* Value | 529.775 |
| *cy* | Y Axis *Principal Points* Value | 411.030 |
| *k1* | Radial Distortion Value | 0.158 |
| *k2* | Radial Distortion Value | -9.925 |
| *k3* | Radial Distortion Value | -32.740 |
| *p1* | Tangential Distortion Value | -0.009 |
| *p2* | Tangential Distortion Value | -0.008 |

**Table 6:** Accuracy assessment of UAV model orthorectification at 20 meters flight altitude

| Points | ICP Coordinates (m) | | Model Coordinates (m) | | Horizontal Accuracy (m) |
|---|---|---|---|---|---|
| | $X_1$ | $Y_1$ | $X_2$ | $Y_2$ | |
| ICP01 | 499105.876 | 9178389.461 | 499105.930 | 9178389.630 | 0.031 |
| ICP02 | 499106.910 | 9178392.265 | 499106.890 | 9178392.400 | 0.019 |
| ICP03 | 499107.254 | 9178388.919 | 499107.650 | 9178389.040 | 0.171 |
| ICP04 | 499090.346 | 9178393.790 | 499090.230 | 9178394.150 | 0.143 |
| ICP05 | 499087.595 | 9178386.083 | 499087.320 | 9178386.180 | 0.085 |
| ICP06 | 499085.827 | 9178373.555 | 499085.770 | 9178373.690 | 0.021 |
| | | | | Total | 0.471 |
| | | | | Mean | 0.280 |
| | | | | RMSE | 0.425 |

**Table 7:** Accuracy assessment of UAV model orthorectification at 30 meters flight altitude

| Points | ICP Coordinates (m) | | Model Coordinates (m) | | Horizontal Accuracy (m) |
|---|---|---|---|---|---|
| | $X_1$ | $Y_1$ | $X_2$ | $Y_2$ | |
| ICP01 | 499105.876 | 9178389.461 | 499106.060 | 9178389.640 | 0.074 |
| ICP02 | 499106.910 | 9178392.265 | 499107.190 | 9178392.400 | 0.097 |
| ICP03 | 499107.254 | 9178388.919 | 499107.530 | 9178389.050 | 0.093 |
| ICP04 | 499090.346 | 9178393.790 | 499090.270 | 9178394.070 | 0.084 |
| ICP05 | 499087.595 | 9178386.083 | 499087.310 | 9178386.120 | 0.083 |
| ICP06 | 499085.827 | 9178373.555 | 499085.560 | 9178373.420 | 0.090 |
| | | | | Total | 0.520 |
| | | | | Mean | 0.294 |
| | | | | RMSE | 0.447 |

**Table 8:** Accuracy assessment of UAV model orthorectification at 50 meters flight altitude

| Points | ICP Coordinates (m) | | Model Coordinates (m) | | Horizontal Accuracy (m) |
|---|---|---|---|---|---|
| | $X_1$ | $Y_1$ | $X_2$ | $Y_2$ | |
| ICP01 | 499105.876 | 9178389.461 | 499105.190 | 9178388.010 | 2.576 |
| ICP02 | 499106.910 | 9178392.265 | 499106.070 | 9178390.360 | 4.335 |
| ICP03 | 499107.254 | 9178388.919 | 499106.580 | 9178387.580 | 2.247 |
| ICP04 | 499090.346 | 9178393.790 | 499089.620 | 9178391.130 | 7.603 |
| ICP05 | 499087.595 | 9178386.083 | 499087.040 | 9178384.070 | 4.360 |
| ICP06 | 499085.827 | 9178373.555 | 499086.070 | 9178373.490 | 0.063 |
| | | | | Total | 21.184 |
| | | | | Mean | 3.531 |
| | | | | RMSE | 1.879 |

*3.3.2 DSLR camera orthorectification result*

The orthorectification test results obtained an RMSE value of 2.929, which can be seen in Figure 6, with details of the accuracy test results in Table 9. Determination of the map class is done by calculating the ICP test RMSE with the formula CE90 = 1.5175 x RMSE Horizontal, resulting in a value of 4.445 so that it can be concluded that the photo quality is included in the third-class map with a scale of 1:10,000.

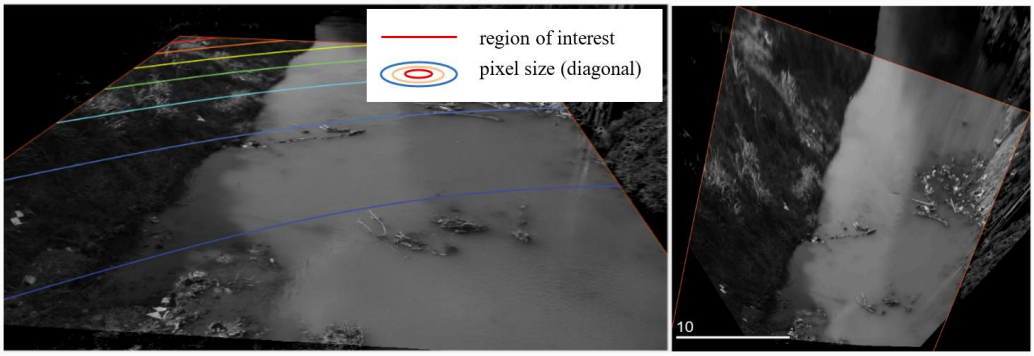


(a) (b)

**Figure 6:** UAV image (a) before orthorectification, and (b) after orthorectification

**Table 9:** Accuracy assessment of camera model orthorectification

| Points | ICP Coordinates (m) | | Model Coordinates (m) | | Horizontal Accuracy (m) |
|---|---|---|---|---|---|
| | $X_1$ | $Y_1$ | $X_2$ | $Y_2$ | |
| ICP01 | 499105.876 | 9178389.461 | 499103.930 | 9178386.390 | 13.218 |
| ICP02 | 499106.910 | 9178392.265 | 499104.050 | 9178388.020 | 26.200 |
| ICP03 | 499107.254 | 9178388.919 | 499104.350 | 9178389.830 | 9.63 |
| ICP04 | 499090.346 | 9178393.790 | 499089.400 | 9178392.950 | 1.601 |
| ICP05 | 499087.595 | 9178386.083 | 499087.090 | 9178386.770 | 0.727 |
| ICP06 | 499085.827 | 9178373.555 | 499086.480 | 9178373.360 | 0.464 |
| | | | | Total | 51.473 |
| | | | | Mean | 8.579 |
| | | | | RMSE | 2.929 |

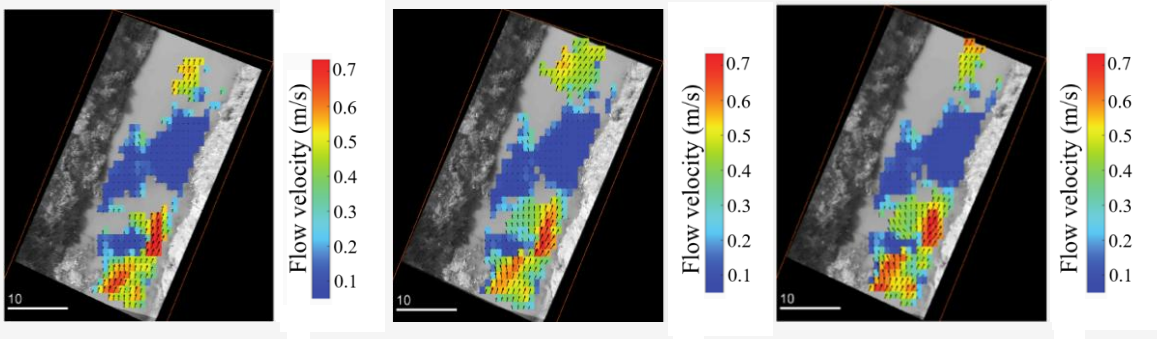


(a) (b) (c)

**Figure 7:** The river flow velocity at a height of 20 m with different data processing time: (a) 120 s – 150 s, (b) 150 s – 180 s, and (c) 180 s – 210 s

*3.4 Flow Velocity Result*

*3.4.1 UAV flow velocity result*

*3.4.1.1 flight altitude 20 meters*

The following is an analysis of river velocity data of the LSPIV method acquired using a UAV with a flying height of 20 meters processed from the results of video data processing seconds 120 to 150, 150 to 180, and 180 to 210. The results of video data processing can be seen in Figure 7. The chart on the right side explains the range of the river flow velocity in m/s, where the blue color represents slow velocity and the red color represents fast velocity. In the middle of the images, it appears that there is a lot of dark blue color, where the waterflow velocity is very slow. These happened because right in the middle of the river, there are a lot of obstacles, such as rocks, sediments, tree branches, and trash. The average velocity is obtained from drawing a cross section in the area where the vector has been calculated, with the results as shown in Figure 7.

*Cross section 1:* obtained an average speed of 0.250 m/s with a speed range of 0.074 m/s to 0.464 m/s and a median of 0.165 m/s in video data processing seconds 120 to 150. Video data processing at seconds 150 to 180 obtained an average speed of 0.287 m/s with a speed range of 0.061 m/s to 0.628 m/s and a median of 0.14 m/s at Cross Section 1. Video data processing at seconds 180 to 210 obtained an average speed of 0.251 m/s with a speed range of 0.052 m/s to 0.533 m/s and a median of 0.128 m/s at Cross Section 1.

*Cross section 2:* obtained an average speed of 0.419 m/s with a speed range of 0.113 m/s to 0.687 m/s and a median of 0.431 m/s in video data processing seconds 120 to 150. Video data processing at seconds 150 to 180 obtained an average speed of 0.454 m/s with a speed range of 0.098 m/s to 0.787 m/s and a median of 0.397 m/s in Cross Section 2. Video data processing at seconds 180 to 210 obtained an average speed of 0.441 m/s with a speed range of 0.09 m/s to 0.806 m/s and a median of 0.401 m/s at Cross Section 2.

*Cross section 3:* obtained an average speed of 0.100 m/s with a speed range of 0.056 m/s to 0.146 m/s and a median of 0.093 m/s in video data processing seconds 120 to 150. Video data processing at seconds 150 to 180 obtained an average speed of 0.155 m/s with a speed range of 0.068 m/s to 0.327 m/s and a median of 0.134 m/s in Cross Section 3. Video data processing at seconds 180 to 210 obtained an average speed of 0.159 m/s with a speed range of 0.053 m/s to 0.293 m/s and a median of 0.138 m/s at Cross Section 3. The average speed is obtained from drawing a cross section in the area where the vector has been calculated, with the results as shown in Figure 8.

*Cross section 4:* obtained an average speed of 0.092 m/s with a speed range of 0.042 m/s to 0.294 m/s and a median of 0.059 m/s at the processing of video data seconds 120 to 150. Video data processing at seconds 150 to 180 obtained an average speed of 0.090 m/s with a speed range of 0.036 m/s to 0.249 m/s and a median of 0.053 m/s at Cross Section 4. Video data processing at seconds 180 to 210 obtained an average speed of 0.090 m/s with a speed range of 0.024 m/s to 0.299 m/s and a median of 0.031 m/s at Cross Section 4. The average velocity is obtained from drawing a cross section in the area where the vector has been calculated, with the results as shown in Figure 8.

*Cross section 5:* obtained an average speed of 0.135 m/s with a speed range of 0.055 m/s to 0.271 m/s and a median of 0.090 m/s on video data processing seconds 120 to 150. Video data processing at seconds 150 to 180 obtained an average speed of 0.129 m/s with a speed range of 0.052 m/s to 0.266 m/s and a median of 0.111 m/s on Cross Section 5. Video data processing at seconds 180 to 210 obtained an average speed of 0.129 m/s with a speed range of 0.04 m/s to 0.235 m/s and a median of 0.145 m/s at Cross Section 5.

Statistical testing using R Studio includes the Kolmogorov-Smirnov normality test and the two-tailed independent t-test for flight altitude 20 meters, where $H_0$: The river flow velocity of the LSPIV method has no significant difference with the river flow validation measurement, and $H_1$: The river flow velocity of the LSPIV method has a significant difference with the river flow validation measurement. Normality testing obtained a p-value of 0.09338, which is larger than the confidence value (a) of 0.05. It means the data is normally distributed. The results of the two-tailed independent t-test with a 95% confidence interval get a t-value of -7.732 and a p-value with 118 degrees of freedom worth $3.9\times10^{-12}$. Since the p-value is smaller than the value of a/2 and the T count value is outside the T table area, it can be determined that $H_1$ is accepted with the conclusion that the river flow velocity of the LSPIV method has a significant difference with the river flow validation measurement.

Figure 8 shows a few 0 values for velocity. This occurs because the velocity cannot be estimated where the water surface is too bright because of the sunlight and over contrast in the image enhancement, so the seeder/tracer cannot be traced. Besides that, the dark spot of the pictures because it was covered with vegetation and rock, and also the river is shallow because of the dry season, makes the tracking even harder. Because the flight altitude is still low, the tracer or seeder can be well determined and calculated.

*3.4.1.2 Flight Altitude 30 Meter*

The following is an analysis of the LSPIV method river velocity data acquired using a UAV with a flight height of 30 meters processed from the results of video data processing seconds 0 to 30, 240 to 270, and 300 to 330. The results of video data processing can be seen in Figure 9. The chart on the right side explains the range of the river flow velocity in m/s, where the blue color represents slow velocity and the red color represents fast velocity.

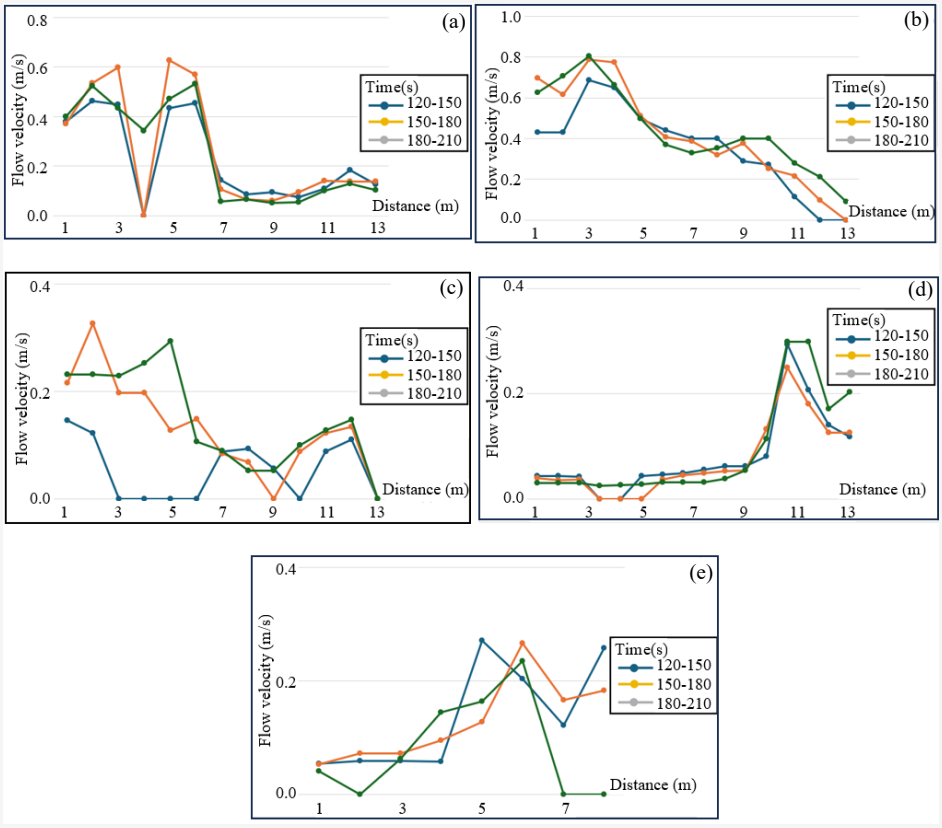


**Figure 8:** The average velocity of the UAV with a flight altitude of 20 meters at different cross section: (a) cross section 1, (b) cross section 2, (c) cross section 3, (d) cross section 4, and (e) cross section 5

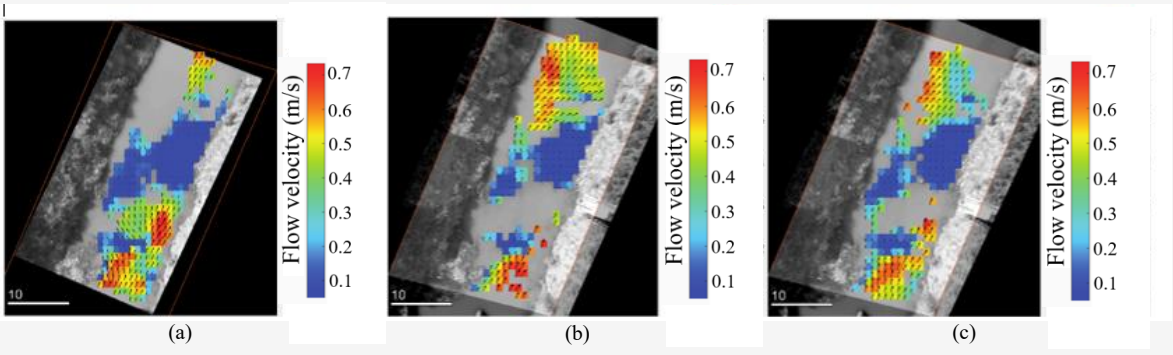


**Figure 9:** The river flow velocity at a height of 30m (m/s) with different data processing time (a) 120 s – 150 s, (b) 150 s – 180 s, and (c) 180 s – 210 s

In the middle of the images, it appears that there is a lot of dark blue color, where the waterflow velocity is very slow. These happened because right in the middle of the river, there are a lot of obstacles, such as rocks, sediments, tree branches, and trash.

*Cross section 1:* obtained an average speed of 0.233 m/s with a speed range of 0.086 m/s to 0.445 m/s and a median of 0.201 m/s on video data processing seconds 0 to 30. Video data processing at seconds 240 to 270 obtained an average speed of 0.253 m/s with a speed range of 0.079 m/s to 0.599 m/s and a median of 0.223 m/s on Cross Section 1. Video data processing at seconds 300 to 330 obtained an average speed of 0.363 m/s with a speed range of 0.094 m/s to 0.643 m/s and a median of 0.241 m/s at Cross Section 1.

*Cross section 2:* obtained an average speed of 0.496 m/s with a speed range of 0.222 m/s to 0.701 m/s and a median of 0.526 m/s at video data processing seconds 0 to 30. Video data processing at seconds

240 to 270 obtained an average speed of 0.268 m/s with a speed range of 0.100 m/s to 0.486 m/s and a median of 0.242 m/s at Cross Section 2. Video data processing at seconds 300 to 330 obtained an average speed of 0.516 m/s with a speed range of 0.252 m/s to 0.696 m/s and a median of 0.548 m/s at Cross Section 2.

*Cross section 3:* obtained an average speed of 0.258 m/s with a speed range of 0.077 m/s to 0.402 m/s and a median of 0.263 m/s in video data processing seconds 0 to 30. Video data processing at seconds 240 to 270 obtained an average speed of 0.231 m/s with a speed range of 0.118 m/s to 0.320 m/s and a median of 0.238 m/s in Cross Section 3. Video data processing at seconds 300 to 330 obtained an average speed of 0.185 m/s with a speed range of 0.101 m/s to 0.250 m/s and a median of 0.201 m/s at Cross Section 3.

*Cross section 4:* obtained an average speed of 0.116 m/s with a speed range of 0.051 m/s to 0.286 m/s and a median of 0.06 m/s on video data processing seconds 0 to 30. Video data processing at seconds 240 to 270 obtained an average speed of 0.135 m/s with a speed range of 0.063 m/s to 0.344 m/s and a median of 0.065 m/s on Cross Section 4. Video data processing at seconds 300 to 330 obtained an average speed of 0.146 m/s with a speed range of 0.072 m/s to 0.400 m/s and a median of 0.079 m/s at Cross Section 4.

*Cross section 5:* obtained an average speed of 0.321 m/s with a speed range of 0.064 m/s to 0.625 m/s and a median of 0.273 m/s on video data processing seconds 0 to 30. Video data processing at seconds 240 to 270 obtained an average speed of 0.311 m/s with a speed range of 0.065 m/s to 0.503 m/s and a median of 0.361 m/s on Cross Section 5. Video data processing at seconds 300 to 330 obtained an average speed of 0.331 m/s with a speed range of 0.078 m/s to 0.598 m/s and a median of 0.264 m/s at Cross Section 5.

Statistical testing using R Studio includes the Kolmogorov-Smirnov normality test and the two-tailed independent t-test for flight altitude of 30 meters, where $H_0$: The river flow velocity of the LSPIV method has no significant difference with the river flow validation measurement, and $H_1$: The river flow velocity of the LSPIV method has a significant difference with the river flow validation measurement. Normality testing obtained a p-value of 0.349, which is larger than the confidence value (a) of 0.05. It means the data is normally distributed. The results of the two-tailed independent t-test with a 95% confidence interval get a t-value of -5.725 and a p-value with 118 degrees of freedom worth $8\times10^{-8}$. Since the p-value is smaller than the value of a/2 and the T count value is outside the T table area, it can be determined that $H_1$ is accepted with the conclusion that the river flow velocity of the LSPIV method has a significant difference with the river flow validation Measurement. Figure 10 explains the surface current velocity values at each cross-section we created, allowing us to see the differences at each point due to various factors within the river. There are many obstacles, such as rocks, sediments, tree branches, and trash, which cause the surface current velocity values to vary.

Figure 10 shows a lot of 0 value on velocity. This occurs because the velocity cannot be estimated where the water surface is too bright because of the sunlight and over contrast in the image enhancement, and the flight altitude was higher. Also, the natural seeder/tracer is too small, so the seeder/tracer cannot be traced. Besides that, the dark spot of the pictures because it was covered with vegetation and rock, and also the river is shallow because of the dry season, makes the tracking even harder.

*3.4.1.3 Flight altitude 50 meters*

The following is an analysis of river velocity data of the LSPIV method acquired using a UAV with a flight height of 50 meters processed from the results of video data processing seconds 240 to 270, 270 to 300, and 330 to 330. The results of video data processing can be seen in Figure 11. The chart on the right side explains the range of the river water flow velocity in m/s, where the blue color represents slow velocity and the red color represents fast velocity. In the middle of the images, it appears that there is a lot of dark blue color, where the waterflow velocity is very slow. These happened because right in the middle of the river, there are a lot of obstacles, such as rocks, sediments, tree branches, and trash. Figure 12 represents the cross-section position to take the velocity sample value. We used three different capture time frames with 30-second intervals. Those are 240s to 270s, 270s to 300s, and 300s to 330s.

*Cross section 1:* obtained an average speed of 0.200 m/s with a speed range of 0.139 m/s to 0.274 m/s. It has a median value of 0.184 m/s in video data processing seconds 240 to 270. Video data processing at seconds 270 to 300 obtained an average speed of 0.229 m/s with a speed range of 0.127 m/s to 0.294 m/s and a median value of 0.241 m/s on Cross Section 1. Video data processing at seconds 300 to 330 obtained an average speed of 0.285 m/s with a speed range of 0.129 m/s to 0.654 m/s and a median of 0.170 m/s.

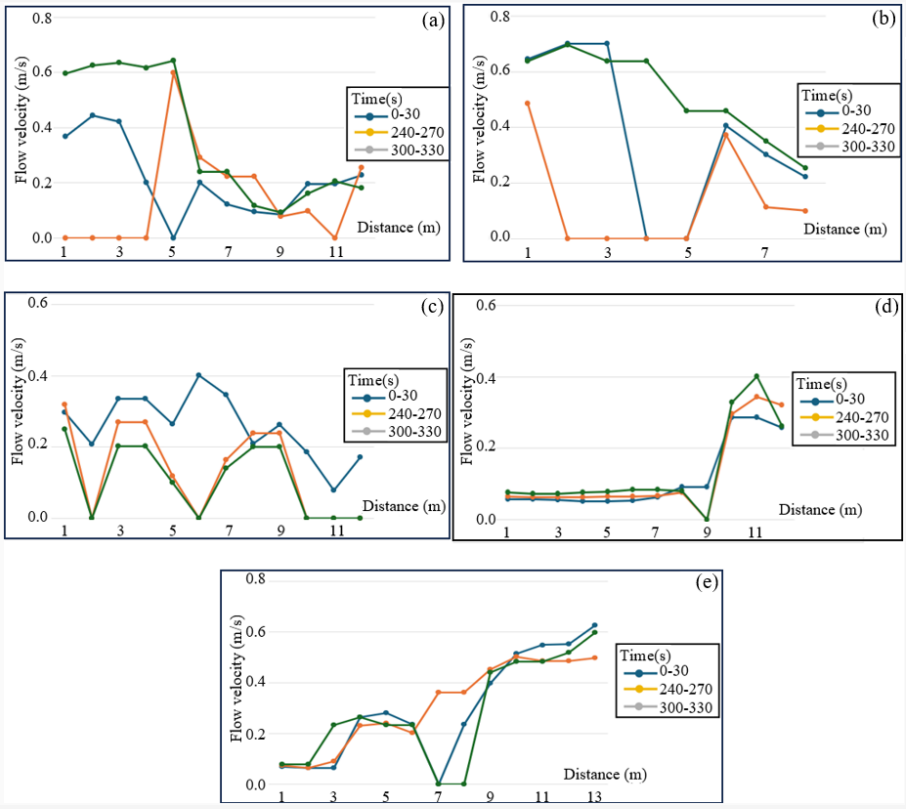


**Figure 10:** The average velocity of the UAV with a flight altitude of 30 meters at different cross section: (a) cross section 1, (b) cross section 2, (c) cross section 3, (d) cross section 4, and (e) cross section 5

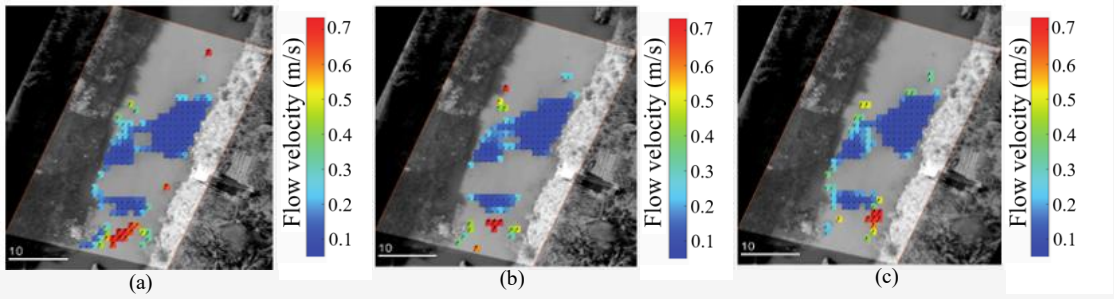


**Figure 11:** The river flow velocity at a height of 50m with different data processing time: (a) 120 s – 150 s, (b) 150 s – 180 s, and (c) 180 s – 210 s

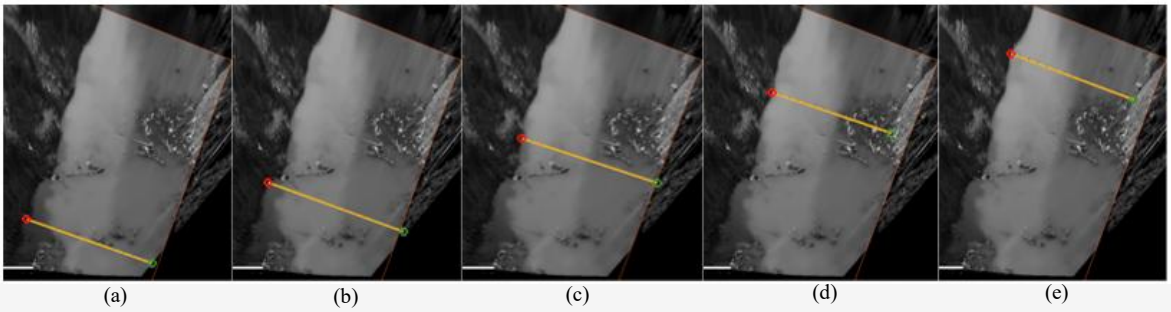


**Figure 12:** UAV-based flow velocity measurement: (a) first cross section, (b) second cross section, (c) third cross section, (d) fourth cross section, (e) fifth cross section. This cross section is used in UAV and camera processing

*Cross section 2:* obtained an average speed of 0.142 m/s with a speed range of 0.135 m/s to 0.146 m/s and a median of 0.146 m/s in video data processing seconds 240 to 270. Video data processing at seconds 300 to 330 obtained an average speed of 0.144 m/s with a speed range of 0.141 m/s to 0.146 m/s and a median of 0.144 m/s in Cross Section 2. Video data processing at seconds 300 to 330 obtained an average speed of 0.170 m/s with a speed of 0.170 m/s.

*Cross section 3:* obtained an average velocity of 0.210 m/s with a velocity range of 0.144 m/s to 0.261 m/s and a median of 0.217 m/s on video data processing seconds 240 to 270. Video data processing at seconds 300 to 330 obtained an average speed of 0.237 m/s with a speed range of 0.193 m/s to 0.281 m/s and a median of 0.221 m/s in Cross Section 3. Video data processing at seconds 300 to 330 obtained an average speed of 0.214 m/s with a speed range of 0.140 m/s to 0.275 m/s and a median of 0.225 m/s.

*Cross section 4:* obtained an average speed of 0.156 m/s with a speed range of 0.106 m/s to 0.406 m/s and a median of 0.126 m/s in video data processing seconds 240 to 270. Video data processing at seconds 270 to 300 obtained an average speed of 0.151 m/s with a speed range of 0.107 m/s to 0.470 m/s and a median of 0.114 m/s on Cross Section 4. Video data processing at seconds 300 to 330 obtained an average speed of 0.153 m/s with a speed range of 0.108 m/s to 0.460 m/s and a median of 0.121 m/s.

*Cross section 5:* obtained an average speed of 0.237 m/s with a speed range of 0.210 m/s to 0.255 m/s and a median of 0.241 m/s in video data processing seconds 240 to 270. Video data processing at seconds 270 to 300 obtained an average speed of 0.280 m/s with a speed range of 0.230 m/s to 0.330m/s and a median of 0.280 m/s at Cross Section 5. Video data processing at seconds 300 to 330 obtained an average speed of 0.243 m/s with a speed range of 0.143 m/s to 0.383 m/s and a median of 0.203 m/s.

Statistical testing using R Studio includes the Kolmogorov-Smirnov normality test and the two-tailed independent t-test for flight altitude of 50 meters, where $H_0$: The river flow velocity of the LSPIV method has no significant difference with the river flow validation measurement, and $H_1$: The river flow velocity of the LSPIV method has a significant difference with the river flow validation measurement. Normality testing obtained a p-value of 0.008, which is smaller than the confidence value (a) of 0.05. It means the data is not normally distributed. But, according to the Central Limit Theorem, since there are more than 60 data observations, it can be concluded that the data is normally distributed. The results of the two-tailed independent t-test with a 95% confidence interval get a t-value of -10.026 and a p-value with 118 degrees of freedom worth $2.2\times10^{-16}$. Since the p-value is smaller than the value of a/2 and the T count value is outside the T table area, it can be determined that $H_1$ is accepted with the conclusion that the river flow velocity of the LSPIV method has a significant difference with the river flow validation measurement. Figure 13 shows a lot of 0 value on velocity. This occurs because the velocity cannot be estimated where the water surface is too bright because of the sunlight and over contrast in the image enhancement, and the flight altitude was higher. Also, the natural seeder/tracer is too small, so the seeder/tracer cannot be traced. Besides that, the dark spot of the pictures because it was covered with vegetation and rock, and also the river is shallow because of the dry season, makes the tracking even harder.

*3.4.2 Camera based flow velocity result*

Calculation of the surface velocity of the river flow in the entire area of the research object gets a range of values of 0-0.7 m/s, with velocity magnitude that can be seen in Figure 14. Calculation of velocity is carried out on five cross sections with details in Figure 15, having each cross section average value of 0.188 m/s, 0.135 m/s, 0.039 m/s, 0.109 m/s, and 0.125 m/s. Comparison of river flow velocities in all cross sections can be seen in the graph in Figure 16. It has the lowest value of 0.0001 m/s on garbage and river sediment and has the largest value of 0.572 m/s on river flow that does not have river sediment obstacles. Statistical testing using R Studio includes the Kolmogorov-Smirnov normality test and the two-tailed independent t-test. Normality testing obtained a p-value of 0.0122, which is smaller than the confidence value (a) of 0.05. However, based on the Central Limit Theorem, since there are more than 60 data observations, it can be concluded that the data is normally distributed. The results of the two-tailed independent t-test with a 95% confidence interval get a t-value of -14.202 and a p-value with 118 degrees of freedom worth $2.2\times10^{-16}$. Since the p-value is smaller than the value of a/2 and the T-value is outside the T-table area, it can be determined that $H_1$ is accepted with the conclusion that the river flow velocity of the LSPIV method has a significant difference with the river flow validation measurement.

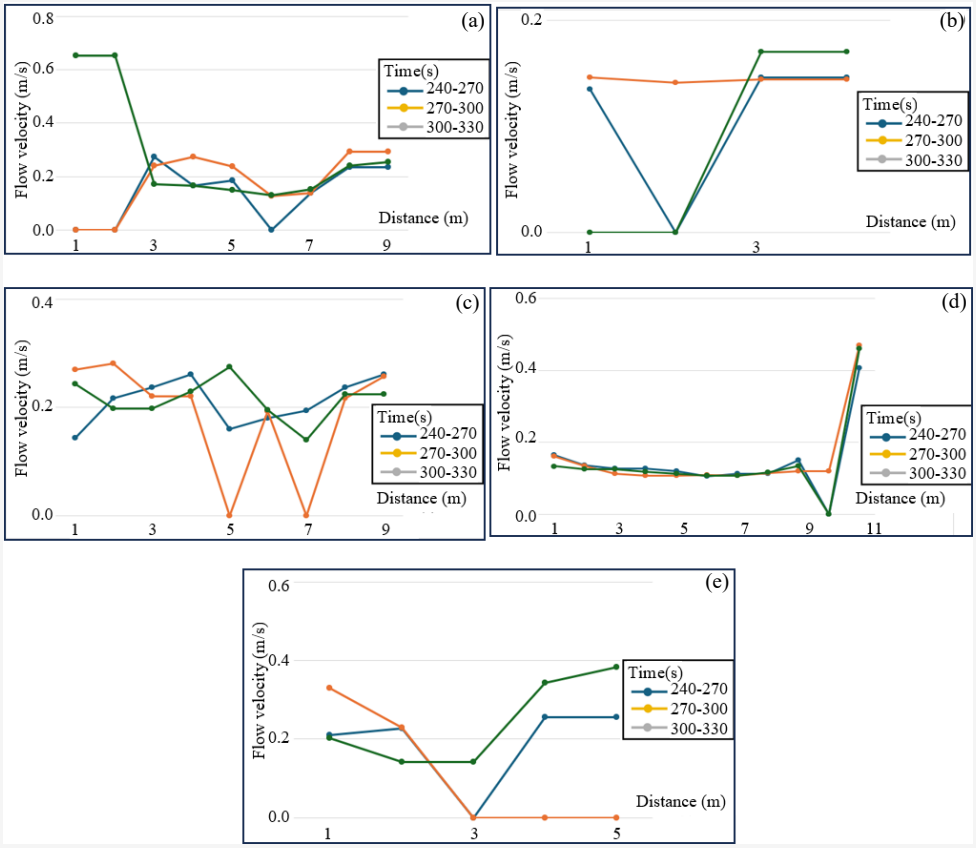


**Figure 13**: The average velocity of the UAV with a flight altitude of 50 meters at different cross section: (a) cross section 1; (b) cross section 2; (c) cross section 3; (d) cross section 4; (e) cross section 5

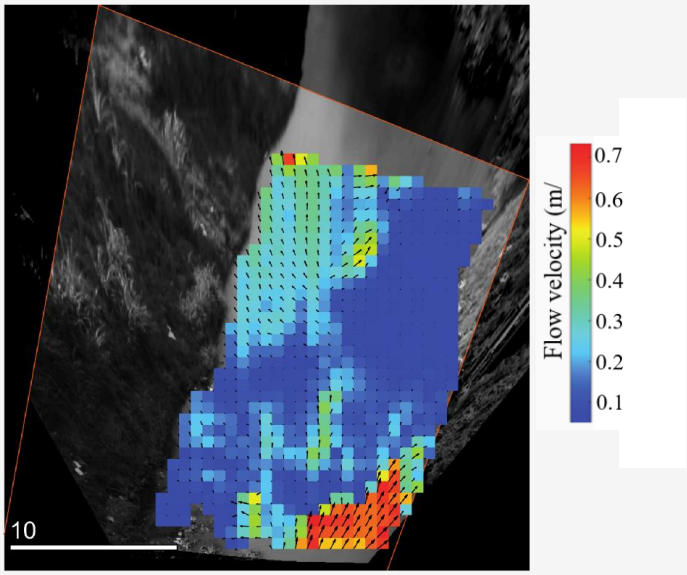


**Figure 14:** The magnitude of the river flow velocity using camera-based (m/s)

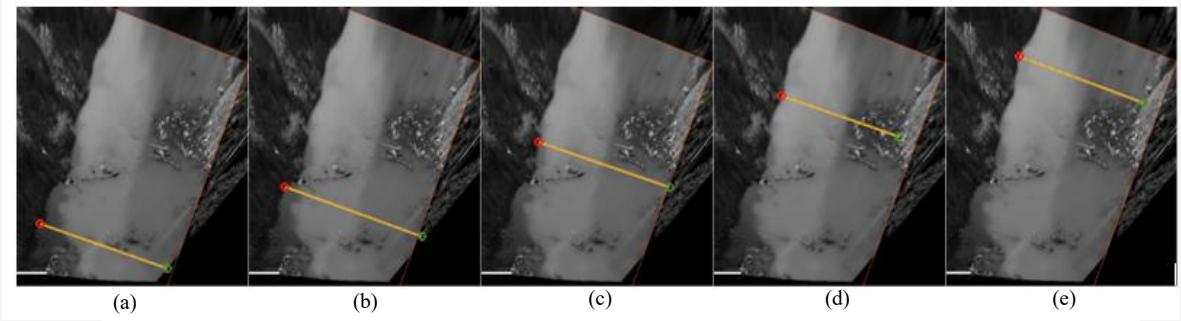


**Figure 15:** Camera-based flow velocity measurement: (a) first cross section; (b) second cross section; (c) third cross section; (d) fourth cross section; (e) fifth cross section

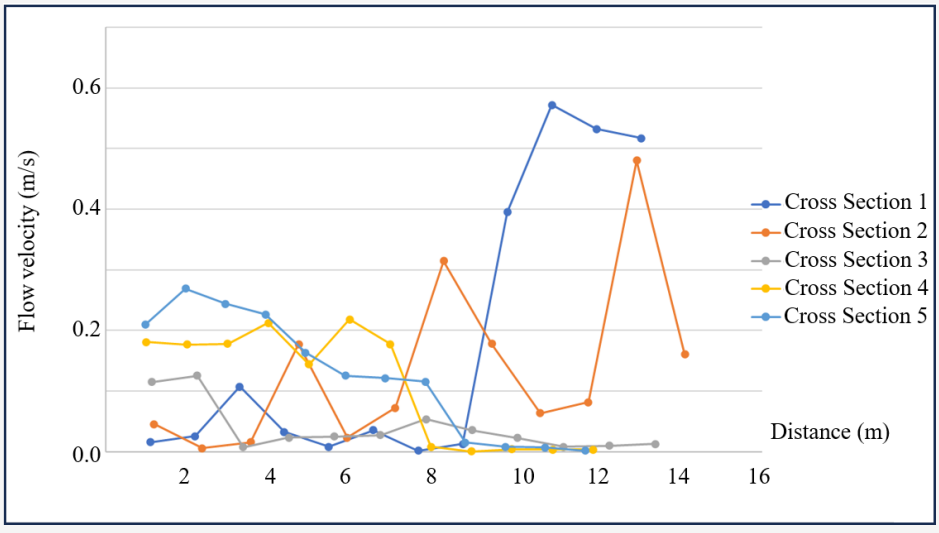


**Figure 16:** The average velocity of camera-based

## 4. Conclusions

This study measured river water discharge using a camera located on a bridge and a UAV in shallow river waters. This study obtained the results of river discharge measurements using the LSPIV technique. The results of river flow velocity measurements using the LSPIV method using a UAV in the Mungkung River produced values of 0.024 to 0.806 m/s for a flight height of 20 meters, 0.051 to 0.701 m/s for a flight height of 30 meters, and 0.106 to 0.654 m/s for a flight height of 50 meters. Meanwhile, the results of acquisition using terrestrial photogrammetry obtained an average value of 0.277 m/s with a value range of 0-0.7 m/s. Meanwhile, Bengawan Solo River Basin Organization data using a current meter produced a velocity value of 0.375 m/s, and field data validation obtained a river water flow velocity of 0.393 m/s. Based on this, the terrestrial photogrammetry method is closer to field data validation compared to UAV. Terrestrial photogrammetry has the advantage of accuracy but must be placed in a stationary position on the earth's surface, while UAVs are more flexible in acquiring data at a certain height and covering a wide area, which can be used to reach high-risk areas. On the other hand, terrestrial photogrammetry only gets good results in areas close to the camera. The further away the area, the greater the distortion, whereas UAVs can minimize the pixel distortion. GCP and ICP should be deployed to expand in the research area. This will help to increase the result of the orthorectification process. The cross section should be given a premark to ease the process in the RIVeR application. Cross-section elevation and depth data can be included for further research to get the water discharge. Also, the water surface elevation has to be measured because the FUDAA-LSPIV needs the data to check the root mean square error of the rectification result. The UAV flight altitude and the camera angle can be concerned in more detail, so the distortion result can be minimum. The river flow velocity must be measured with a current meter in the cross-section area so the result can be more detailed.

**References**


[1] Guillén, N. F., Patalano, A., García, C. M. and Bertoni, J. C., (2017). Use of LSPIV in Assessing Urban Flash Flood Vulnerability. *Natural Hazards,* Vol. 87(1), 383–394. https://doi.org/10.1007/s11069-017-2768-8.

[2] Trieu, H., Bergström, P., Sjödahl. M., Hellström, J. G. I., Andreasson, P. and Lycksam, H., (2021). Photogrammetry for Free Surface Flow Velocity Measurement: From Laboratory to Field Measurements, Water. Vol. 13(12), 1-14. https://doi.org/10.3390/w13121675.

[3] Herschy, R., (1995). General Purpose Flow Measurement Equations for Flumes and Thin Plate Weirs. *Flow Measurement and Instrumentation,* Vol. 6(4), 283-293. https://doi.org/10.1016/0955-5986(95)00016-X.

[4] Sharif, O., (2022). *Measuring Surface Water Flow Velocities by a Drone and Large-Scale Particle Image Velocimetry (LSPIV)*. University of Twente, August.

[5] Alongi, F., Pumo, D., Nasello, C., Nizza, S., Ciraolo, G. and Noto, L. V., (2023). An Automatic ANN-Based Procedure for Detecting Optimal Image Sequences Supporting LS-PIV Applications for Rivers Monitoring. *Journal of Hydrology,* Vol. 626. https://doi.org/10.1016/j.jhydrol.2023.130233.

[6] Gharahjeh, S. and Aydin, I., (2016). Application of Video Imagery Techniques for Low Cost Measurement of Water Surface Velocity in Open Channels. *Flow Measurement and Instrumentation,* Vol. 51, 79–94. https://doi.org/10.1016/j.flowmeasinst.2016.09.001.

[7] Patalano, A., García, C. M. and Rodríguez, A., (2017). Rectification of Image Velocity Results (RIVeR): A Simple and User-Friendly Toolbox for Large Scale Water Surface Particle Image Velocimetry (PIV) and Particle Tracking Velocimetry (PTV). *Computers & Geosciences,* Vol. 109, 323–330. https://doi.org/10.1016/j.cageo.2017.07.009.

[8] Ioli, F., Pinto, L., Passoni, D., Nova, V. and Detert, M., (2020). Evaluation of Airborne Image Velocimetry Approaches Using Low-Cost UAVs in Riverine Environments. *The International Archives of the Photogrammetry, Remote Sensing and Spatial Information Sciences.* Vol. XLIII-B2-2020, 597–604. https://doi.org/10.5194/isprs-archives-XLIII-B2-2020-597-2020.

[9] LeGrand, M. C. L., Luce, J. J., Metcalfe, R. A. and Buttle, J. M., (2020). Development of An Inexpensive Automated Streamflow Monitoring System. *Hydrological Processes,* Vol. 34(13), 3021–3023. https://doi.org/10.1002/hyp.13783.

[10] Detert, M., Johnson, E. D. and Weitbrecht, V., (2017). Proof-of-Concept for Low-Cost and Non-Contact Synoptic Airborne River Flow Measurements. *International Journal of Remote Sensing,* Vol. 38(8–10), 2780–2807. https://doi.org/10.1080/01431161.2017.1294782.

[11] Kim, Y., (2006). *Uncertainty Analysis for Non-Intrusive Measurement of River Discharge Using Image Velocimetry.* Doctoral Dissertation. Civil and Environmental Engineering. The University of Iowa.

[12] Abdulwahab, M. R., Ali, Y. H., Habeeb, F. J., Borhana, A. A., Abdelrhman, A. M. and Al-Obaidi, S. M. A., (2020). A Review in Particle Image Velocimetry Techniques (Developments and Applications). *Journal of Advanced Research in Fluid Mechanics and Thermal Science*, Vol. 65 (2), 213–229. https://www.akademiabaru.com/doc/ARFMTSV65_N2_P213_229.pdf.

[13] Rahardjo, A. P., Burdiarto, R. and Prabowo, I. E., (2011). *Pengembangan Particle Image Velocimetry (PIV) Berbasis Pengolahan Citra untuk Pengukuran Aliran 2D [Development of Image Processing-Based Particle Image Velocimetry (PIV) for 2D Flow Measurement].* Towards Sustainable Engineering. Yogyakarta. Indonesia. Universitas Gadjah Mada.

[14] Bouguet, J. Y. and Perona, P., (1998). Camera Calibration from Points and Lines in Dual-Space Geometry. *Proceeding 5th Europen Conference on Computer Vision*. 1–16.

[15] Liu, W. C., Huang, W. C. and Young, C. C., (2023). Uncertainty Analysis for Image-Based Streamflow Measurement: The Influence of Ground Control Points. *Water,* Vol. 15(1), 1-23. https://doi.org/10.3390/w15010123.

[16] Hauet, A., Creutin, J. D. and Belleudy, P., (2008). Sensitivity Study of Large-Scale Particle Image Velocimetry Measurement of River Discharge Using Numerical Simulation. *Journal of Hydrology,* Vol. 349(1–2), 178–190. https://doi.org/10.1016/j.jhydrol.2007.10.062.

[17] Jolley, M. J., Russell, A. J., Quinn, P. F. and Perks, M. T., (2021). Considerations When Applying Large-Scale PIV and PTV for Determining River Flow Velocity. *Frontiers in Water,* Vol. 3, 1–21. https://doi.org/10.3389/frwa.2021.709269.

[18] Tauro, F., Piscopia, R. and Grimaldi, S., (2019). PTV-Stream: A Simplified Particle Tracking Velocimetry Framework for Stream Surface Flow Monitoring. *Catena,* Vol. 172, 378–386. https://doi.org/10.1016/j.catena.2018.09.009.

[19] Tauro, F., Pagano, C., Phamduy, P., Grimaldi, S. and Porfiri, M., (2015). Large-Scale Particle Image Velocimetry from an Unmanned Aerial Vehicle. *IEEE/ASME Transactions on Mechatronics,* Vol. 20(6), 3269–3275. https://doi.org/10.1109/TMECH.2015.2408112.

[20] Muste, M., Fujita, I. and Hauet, A., (2008). Large-Scale Particle Image Velocimetry for Measurements in Riverine Environments. *Water Resources Research,* Vol. 44(4). https://doi.org/10.1029/2008WR006950.

[21] Mulatsih, U. S. and Sundoro, G. H., (2012). Studi Kasus Kerusakan Pelindung Tebing Sungai Geocell Di Kali Mungkung Desa Patihan Kabupaten Sragen [Case Study of Geocell Riverbank Protection Damage in Mungkung River, Patihan Village, Sragen Regency]. *Jurnal Teknik Hidraulik,* Vol. 3(2), 143–156. https://dx.doi.org/10.32679/jth.v3i2.268.

[22] Thielicke, W. and Stamhuis, E. J., (2014). PIVlab–Towards User-friendly, Affordable and Accurate Digital Particle Image Velocimetry in MATLAB. *Journal Open Research Software,* Vol. 2(1), 1-10. https://doi.org/10.5334/jors.bl.

[23] Masafu, C., Williams, R., Shi, X., Yuan, Q. and Trigg, M., (2022). Unpiloted Aerial Vehicle (UAV) Image Velocimetry for Validation of Two-Dimensional Hydraulic Model Simulations. *Journal Hydrology,* Vol. 612, 1-14. https://doi.org/10.1016/j.jhydrol.2022.128217.

[24] Strelnikova, D., Paulus, G., Käfer, S., Anders, K., Mayr, P., Mader, H., Scherling, U. and Schneeberger, R., (2020). Drone-Based Optical Measurements of Heterogeneous Surface Velocity Fields Around Fish Passages at Hydropower Dams, *Remote Sensing,* Vol. 12(3), 1–25. https://doi.org/10.3390/rs12030384.

[25] Fujita, I., Muste, M. and Kruger, A., (1998). Large-Scale Particle Image Velocimetry for Flow Analysis in Hydraulic Engineering Applications. *Journal of Hydraulic Research,* Vol. 36(3), 397–414. https://doi.org/10.1080/00221689809498626.